Multipolar analysis of second-harmonic radiation from gold nanoparticles

Sami Kujala[1*], **Brian K. Canfield**[1,3], **Martti Kauranen**[1], **Yuri Svirko**[2], **Jari Turunen**[2]

[1]*Optics Laboratory, Institute of Physics, Tampere University of Technology. P.O. Box 692, FI-33101 Tampere, Finland*

[2]*Department of Physics and Mathematics, University of Joensuu, P.O. Box 111, FI-80101 Joensuu, Finland*

[3]*Current address: University of Tennessee Space Institute, MS 24, 411 B. H. Goethert Parkway, Tullahoma, TN 37388*

sami.kujala@tut.fi

Abstract: We present a multipolar tensor analysis of second-harmonic radiation from arrays of noncentrosymmetric L-shaped gold nanoparticles. Our approach is based on the fundamental differences in the radiative properties of electric dipoles and higher multipoles, which give rise to differences in the nonlinear response tensors for the reflected and transmitted second-harmonic signals. The results are analyzed by dividing the tensors into symmetric (dipolar) and antisymmetric (higher multipolar) parts between the two directions. The nonlinear response is found to be dominated by a tensor component, not resolved earlier [Kujala *et. al*, Phys. Rev. Lett. **98**, 167403, (2007)], which is associated with chiral symmetry breaking of the sample and which also contains a strong multipolar contribution. The results are explained by a phenomenological model where asymmetrically-distributed defects on opposite sides of the particles give rise to dipolar and quadrupolar second-harmonic emission.

© 2008 Optical Society of America

OCIS codes: (190.0190) Nonlinear Optics; (310.6628) Subwavelength structures, nanostructures; (260.3910) Metals, optics of

References and links

1. U. Kreibig and M. Vollmer, *Optical Properties of Metal Clusters*, Springer Series in Materials Science (Springer, Berlin, 1995).
2. A. Christ, T. Zentgraf, J. Kuhl, S. G. Tikhodeev, N. A. Gippius, and H. Giessen, "Optical properties of planar metallic photonic crystal structures: Experiment and theory," Phys. Rev. B **70**, 125113 (2004).
3. S. Zou, N. Janel, and G. C. Schatz, "Silver nanoparticle array structures that produce remarkably narrow plasmon lineshapes," J. Chem. Phys. **120**, 10,871–10,875 (2004).
4. T. Vallius, K. Jefimovs, J. Turunen, P. Vahimaa, and Y. Svirko, "Optical activity in subwavelength-period arrays of chiral metallic particles," Appl. Phys. Lett. **83**, 234 (2003).
5. T. Y. F. Tsang, "Surface-plasmon-enhanced third-harmonic generation in thin silver films," Opt. Lett. **21**, 245 (1996).
6. N. Félidj, J. Aubard, G. Lévi, J. R. Krenn, M. Salerno, G. Schider, B. Lamprecht, A. Leitner, and F. R. Aussenegg, "Controlling the optical response of regular arrays of gold particles for surface-enhanced Raman scattering," Phys. Rev. B **65**, 075,419 (2002).
7. A. Bouhelier, M. Beversluis, A. Hartschuh, and L. Novotny, "Near-Field Second-Harmonic Generation Induced by Local Field Enhancement," Phys. Rev. Lett. **90**, 013,903 (2003).

#97124 - $15.00 USD Received 6 Jun 2008; revised 6 Oct 2008; accepted 7 Oct 2008; published 13 Oct 2008

8. M. I. Stockman, D. J. Bergman, and T. Kobayashi, "Coherent control of nanoscale localization of ultrafast optical excitation in nanosystems," Phys. Rev. B **69**, 054,202 (2004).
9. L. H. Qian, X. Q. Yan, T. Fujita, A. Inoue, and M. W. Chena, "Surface enhanced Raman scattering of nanoporous gold: Smaller pore sizes stronger enhancements," Appl. Phys. Lett. **90**, 153,120 (2007).
10. B. K. Canfield, H. Husu, J. Laukkanen, B. Bai, M. Kuittinen, J. Turunen, and M. Kauranen, "Local Field Asymmetry Drives Second-Harmonic Generation in Noncentrosymmetric Nanodimers," Nano Lett. **7**, 1251–1255 (2007).
11. P. Guyot-Sionnest, W. Chen, and Y. Shen, "General considerations on optical second-harmonic generation from surfaces and interfaces," Phys. Rev. B **33**, 8254–8263 (1986).
12. M. Kauranen, T. Verbiest, J. J. Maki, and A. Persoons, "Second-harmonic generation from chiral surfaces," J. Chem. Phys. **101**, 8193 (1994).
13. M. Kauranen, J. J. Maki, T. Verbiest, S. V. Elshocht, and A. Persoons, "Quantitative determination of electric and magnetic second-order susceptibility tensors of chiral surfaces," Phys. Rev. B **55**, R1985 (1997).
14. S. V. Elshocht, T. Verbiest, M. Kauranen, A. Persoons, B. M. W. Langeveld-Voss, and E. W. Meijer, "Direct evidence of the failure of electric-dipole approximation in second-harmonic generation from a chiral polymer film," J. Chem. Phys. **107**, 8201–8203 (1997).
15. F. Hache, H. Mesnil, and M. C. Schanne-Klein, "Nonlinear circular dichroism in a liquid of chiral molecules: A theoretical investigation," Phys. Rev. B **60**, 6405–6411 (1999).
16. M. C. Schanne-Klein, F. Hache, T. Brotin, C. Andraud, and A. Collet, "Magnetic chiroptical effects in surface second harmonic reflection," Chem. Phys. Lett. **338**, 159–166 (2001).
17. C. F. Bohren and D. R. Huffman, *Absorption and Scattering of Light by Small Particles* (John Wiley & Sons, Inc., 1983).
18. S. J. Oldenburg, G. D. Hale, J. B. Jackson, and N. J. Halas, "Light scattering from dipole and quadrupole nanoshell antennas," Appl. Phys. Lett. **75**, 1063 (1999).
19. J. Krenn, G. Schider, W. Rechberger, B. Lamprecht, F. Leitner, A. Aussenegg, and J. Weeber, "Design of multipolar plasmon excitations in silver nanoparticles," Appl. Phys. Lett. **77**, 3379 (2000).
20. K. L. Kelly, E. Coronado, L. L. Zhao, and G. C. Schatz, "The Optical Properties of Metal Nanoparticles: The Influence of Size, Shape, and Dielectric Environment," J. Phys. Chem B **107**, 668 (2003).
21. L. Gunnarsson, T. Rindzevicius, J. Prikulis, B. Kasemo, M. Käll, S. Zou, and G. C. Schatz, "Confined Plasmons in Nanofabricated Single Silver Particle Pairs: Experimental Observations of Strong Interparticle Interactions," J. Phys. Chem. B **109**, 1079–1087 (2005).
22. J. E. Millstone, S. Park, K. L. Shuford, L. D. Qin, G. C. Schatz, and C. A. Mirkin, "Observation of a quadrupole plasmon mode for a colloidal solution of gold nanoprisms," J. Am. Chem. Soc. **127**, 5312 (2005).
23. K. L. Shuford, M. A. Ratner, and G. C. Schatz, "Multipolar excitation in triangular nanoprisms," J. Chem. Phys. **123**, 114713 (2005).
24. R. Bukasov and J. S. Shumaker-Parry, "Highly Tunable Infrared Extinction Properties of Gold Nanocrescents," Nano Lett. **7**, 1113–1118 (2007).
25. A. K. Sheridan, A. W. Clark, A. Glidle, J. M. Cooper, and D. R. S. Cumming, "Multiple plasmon resonances from gold nanostructures," Appl. Phys. Lett. **90**, 143105 (2007).
26. L. Cao, N. C. Panoiu, and R. M. J. Osgood, "Surface second-harmonic generation from surface plasmon waves scattered by metallic nanostructures," Phys. Rev. B **75**, 205,401 (2007).
27. Y. Zhang, B. Fluegel, and A. Mascarenhas, "Total Negative Refraction in Real Crystals for Ballistic Electrons and Light," Phys. Rev. Lett. **91**, 157,404 (2003).
28. D. R. Smith, J. B. Pendry, and M. C. K. Wiltshire, "Metamaterials and Negative Refractive Index," Science **305**, 788–792 (2004).
29. C. Enkrich, M. Wegener, S. Linden, S. Burger, L. Zschiedrich, F. Schmidt, J. F. Zhou, T. Koschny, and C. M. Soukoulis, "Magnetic Metamaterials at Telecommunication and Visible Frequencies," Phys. Rev. Lett. **95**, 203,901 (2005).
30. V. Shalaev, W. Cai, U. Chettiar, H. Yuan, A. Sarychev, V. Drachev, and A. Kildishev, "Negative index of refraction in optical metamaterials," Opt. Lett. **30**, 3356–3358 (2005).
31. T. Pakizeh, M. S. Abrishamian, N. Granpayeh, A. Dmitriev, and M. Käll, "Magnetic-field enhancement in gold nanosandwiches," Opt. Express **14**, 8240–8246 (2006).
32. M. W. Klein, C. Enkrich, M. Wegener, and S. Linden, "Second-Harmonic Generation from Magnetic Metamaterials," Science **313**, 502–504 (2006).
33. M. W. Klein, M. Wegener, N. Feth, and S. Linden, "Experiments on second- and third-harmonic generation from magnetic metamaterials," Opt. Express **15**, 5238–5247 (2007).
34. C. Rockstuhl, F. Lederer, C. Etrich, T. Zentgraf, J. Kuhl, and H. Giessen, "On the reinterpretation of resonances in split-ring-resonators at normal incidence," Opt. Express **14**, 8827–8836 (2006).
35. V. L. Brudny, W. L. Mochán, J. A. Maytorena, and B. S. Mendoza, "Second harmonic generation from a collection of nanoparticles," Phys. Status Solidi B **240**, 518–526 (2003).
36. J. I. Dadap, J. Shan, and T. F. Heinz, "Theory of optical second-harmonic generation from a sphere of centrosymmetric material: small-particle limit," J. Opt. Soc. Am. B **21**, 1328 (2004).

#97124 - $15.00 USD Received 6 Jun 2008; revised 6 Oct 2008; accepted 7 Oct 2008; published 13 Oct 2008
(C) 2008 OSA

37. J. Shan, J. I. Dadap, I. Stiopkin, G. A. Reider, and T. F. Heinz, "Experimental study of optical second-harmonic scattering from spherical nanoparticles," Phys Rev. A **73**, 023,819 (2006).
38. J. Nappa, I. Russier-Antoine, E. Benichou, C. Jonin, and P.-F. Brevet, "Wavelength dependence of the retardation effects in silver nanoparticles followed by polarization resolved hyper Rayleigh scattering," Chem. Phys. Lett. **415**, 246 (2005).
39. J. Nappa, G. Revillod, I. Russier-Antoine, E. Benichou, C. Jonin, and P. F. Brevet, "Electric dipole origin of the second harmonic generation of small metallic particles," Phys. Rev. B **71**, 165,407 (2005).
40. J. Nappa, I. Russier-Antoine, E. Benichou, C. Jonin, and P. F. Brevet, "Second harmonic generation from small gold metallic particles: From the dipolar to the quadrupolar response," J. Chem. Phys. **125**, 184,712 (2006).
41. J. I. Dadap, J. Shan, K. B. Eisenthal, and T. F. Heinz, "Second-Harmonic Rayleigh Scattering from a Sphere of Centrosymmetric Material," Phys. Rev. Lett. **83**, 4045 (1999).
42. L. Li, "Fourier modal method for crossed anisotropic gratings with arbitrary permittivity and permeability tensors," J. Opt. A: Pure Appl. Opt **5**, 345–355 (2003).
43. C. I. Valencia, E. R. Méndez, and B. S. Mendoza, "Second-harmonic generation in the scattering of light by two-dimensional particles," J. Opt. Soc. Am. B **20**, 2150–2161 (2003).
44. L. Li, "New formulation of the Fourier modal method for crossed surface-relief gratings," J. Opt. Soc. Am. A **14**, 2758–2767 (1997).
45. B. Bai and J. Turunen, "Fourier modal method for the analysis of second-harmonic generation in two-dimensionally periodic structures containing anisotropic materials," J. Opt. Soc. Am. B **24**, 1105–1112 (2007).
46. H. Tuovinen, M. Kauranen, K. Jefimovs, P. Vahimaa, T. Vallius, J. Turunen, N. V. Tkachenko, and H. Lemmetyinen, "Linear and second-order nonlinear optical properties of arrays of noncentrosymmetric gold nanoparticles," J. Nonlinear Opt. Phys. **11**, 421 (2002).
47. S. Kujala, B. K. Canfield, M. Kauranen, Y. Svirko, and J. Turunen, "Multipole Interference in the Second-Harmonic Optical Radiation from Gold Nanoparticles," Phys. Rev. Lett. **98**, 167403 (2007). Featured in April 30, 2007 issue of Virtual Journal of Nanoscale Science & Technology **15**, (2007).
48. B. K. Canfield, S. Kujala, K. Laiho, K. Jefimovs, J. Turunen, and M. Kauranen, "Chirality arising from small defects in gold nanoparticle arrays," Opt. Express **14**, 950 (2006).
49. B. K. Canfield, S. Kujala, K. Jefimovs, Y. Svirko, J. Turunen, and M. Kauranen, "A macroscopic formalism to describe the second-order nonlinear optical response of nanostructures," J. Opt. A: Pure Appl. Opt **8**, S278 (2006).
50. R. W. Boyd, *Nonlinear Optics*, 2nd ed. (Academic Press, 2003).
51. M. I. Stockman, D. J. Bergman, C. Anceau, S. Brasselet, and J. Zyss, "Enhanced Second-Harmonic Generation by Metal Surfaces with Nanoscale Roughness: Nanoscale Dephasing, Depolarization, and Correlations," Phys. Rev. Lett. **92**, 057402 (2004).
52. K. Li, M. I. Stockman, and D. J. Bergman, "Enhanced second harmonic generation in a self-similar chain of metal nanospheres," Phys. Rev. B **72**, 153,401 (2005).
53. F. X. Wang, M. Siltanen, and M. Kauranen, "Uniqueness of determination of second-order nonlinear optical expansion coefficients of thin films," Phys. Rev. B **76**, 085428 (2007).
54. W. H. Press, S. A. Teukolsky, W. T. Vetterling, and B. P. Flannery, *Numerical Recipes in Fortran: the art of scientific computing*, 2nd ed. (Cambridge University Press, 1997).
55. M. Born and E. Wolf, *Principles of Optics*, 7th ed. (Cambridge University Press, 1999).
56. B. K. Canfield, S. Kujala, K. Jefimovs, T. Vallius, J. Turunen, and M. Kauranen, "Remarkable Polarization Sensitivity of Gold Nanoparticle Arrays," Appl. Phys. Lett. **86**, 183,109 (2005).

1. Introduction

The optical properties of metal nanoparticles are dominated by plasmon resonances which arise from collective oscillations of conduction electrons [1]. The resonances depend sensitively on the size and shape of the particles and on their dielectric environment. For particles organized in an array on a substrate, the mutual ordering of the particles also plays an important role, and the resonances can be further influenced by Wood anomalies [2, 3] or waveguide modes [4]. The resonances are associated with strong local electromagnetic fields near the particles. Such locally-enhanced fields are particularly interesting for nonlinear optical effects that scale with a high power of the field [5, 6, 7, 8, 9, 10]. Nanoscale variations in the fields, material properties, and nonlinear sources lead to strong gradients in these quantities, which may in turn be favorable for nonlinearities due to higher multipole (magnetic-dipole, electric-quadrupoles, etc.) effects [11]. However, the precise role of different multipolar contributions to the nonlinear responses of nanoparticles has not been explored in detail.

#97124 - $15.00 USD Received 6 Jun 2008; revised 6 Oct 2008; accepted 7 Oct 2008; published 13 Oct 2008
(C) 2008 OSA

One needs to distinguish between two different types of multipoles when discussing the nonlinear responses of nanostructured materials. The first type arises from the light-matter interaction Hamiltonian and corresponds to microscopic multipole moments on the atomic or molecular level. Such multipoles can enable second-order nonlinear effects from centrosymmetric materials [11], which are forbidden within the electric-dipole approximation of the light-matter interaction. In addition, the role of magnetic interactions in the nonlinear response of thin films of chiral molecules has been discussed extensively [12, 13, 14, 15, 16].

The second type of multipoles arises from Mie scattering theory [17]. The standard Mie theory is based on a dipolar microscopic interaction, and effective multipoles arise from size and retardation effects. Usually, the optical responses of particles that are small compared to the wavelength can be described in terms of electric dipoles only [1]. However, when the particle size approaches the wavelength, the dipolar picture may no longer provide a complete description, and higher multipoles should also be considered. Both microscopic and effective multipoles, however, lead to similar radiation patterns in the far field.

The contribution of multipoles to the linear optical responses of metal nanoparticles has been discussed in the literature [18, 19, 20, 21, 22, 23, 24, 25]. For example, metallic nanoshells can be driven selectively into dipolar and quadrupolar oscillation patterns [18]. Size-dependence of multipolar plasmon resonances from elongated silver nanoparticles has also been studied [19], and predictions of the multipolar character of charge density distributions in triangular nanoprisms have been published [23]. Nonlinearities driven by propagating surface plasmon polaritons have also been discussed in terms of multipolar effects [26].

Magnetic resonances are becoming important also for metamaterials, with a negative index of refraction [27, 28, 29, 30, 31]. The nonlinear properties of split-ring resonators have been demonstrated, and a new mechanism proposed to explain the results [32, 33]. Both second- and third-harmonic responses from such resonators were enhanced near the magnetic resonance. The second-harmonic (SH) response was explained by assuming that the fundamental field drives both the magnetic resonance, which gives rise to a strong magnetic field, and the velocity of electrons. The coupling between the magnetic field and the electron motion through the Lorentz force then gives rise to dipolar SH radiation. The magnetic excitation therefore acts as a kind of a local-field effect, whereas the fundamental couplings between the radiation fields and the resonances occur through dipolar mechanisms. The local-field aspect is further emphasized by the fact that the split-ring resonators can also be discussed in terms of plasmon resonances of different orders [34].

A first-principles microscopic theory of the nonlinear properties of nanoscale particles of arbitrary shape is still lacking, although SH (hyper-Rayleigh) scattering from particles of high symmetry has been discussed [35, 36]. Conventional approach usually relies on phenomenological description of the nonlinear response, but the results suggest that both microscopic and Mie-type multipole effects can be important. Experimental evidence of such effects has also been reported [37]. In addition, retardation effects in hyper-Rayleigh scattering from 20-80 nm gold and silver spheres [38, 39, 40] have been observed. The responses from the smallest particles could be explained using the dipolar picture. The responses of larger particles, however, required the inclusion of quadrupolar contributions associated with retardation effects due to nonlocal excitation of surface nonlinearities.

While no true first-principles microscopic theory of the nonlinear properties of nanoscale particles exists yet, the concept is clear – one needs to keep track of the nanoscale variations in the electromagnetic fields, material properties, and nonlinear sources and then integrate the nonlinear responses over the entire structure. There are several phenomenological treatises along these lines on SH scattering [41, 42, 43, 35, 36], in particular, for particles of high symmetry. In practice however, precisely modeling the microscopic and macroscopic nonlinear responses of

#97124 - $15.00 USD Received 6 Jun 2008; revised 6 Oct 2008; accepted 7 Oct 2008; published 13 Oct 2008
(C) 2008 OSA

arbitrarily-shaped and arranged nanoparticles, even on a phenomenological level, is exceptionally difficult. There is some progress in numerical work, though. Recently, numerical results for second-harmonic generation (SHG) from two-dimensional periodic structures, based on the Fourier modal method [44], have been demonstrated [45]. Although the nonlinear response was described in a greatly simplified way, the results were in qualitative agreement with the experiment of Ref. [46] regarding the role of particle ordering.

We have recently provided direct evidence of significant multipolar emission in SHG from an array of L-shaped gold nanoparticles [47]. The evidence is based on the different radiative properties of electric-dipole sources vs. magnetic-dipole and electric-quadrupole sources in two opposite directions. By relying on the dependence of the excitation of different types of sources on the polarization of the fundamental field, and comparing the transmitted and reflected SH signals, we found that the higher-multipole effects accounted for up to 20% of the amplitude of the emitted SH field. The sample investigated had earlier been shown to exhibit chiral symmetry breaking due to its small-scale defects [48] and the strongest multipole effects were associated with signals that arise from this symmetry breaking.

In this Paper, we present a more complete multipolar tensor analysis of the SH response of the sample investigated in Ref. [47]. Our analysis separates the dipolar and higher-multipolar parts of all in-plane components of the nonlinear response tensor [49]. In addition to reaffirming the earlier result [47], we find that the nonlinear response is dominated by one tensor component, not resolved earlier, which is associated with chiral symmetry breaking and exhibits a strong multipolar contribution to the response. The results are interpreted by a phenomenological model where dipolar and quadrupolar SH emission arises from interference between retarded SH wavelets emitted from non-equivalent defects located at laterally opposite sides of the particles.

2. Theoretical background

Traditionally, macroscopic second-order responses are described using the susceptibility tensor $\chi^{(2)}$, which connects the driving fields and the nonlinear source polarization. The tensor is obtained by assuming that the material is homogeneous on a scale larger than molecules (or atoms) but smaller than wavelength and by averaging the molecular responses over such scale. The nanoscopic local electric fields are assumed to be proportional to the macroscopic fields, differing only by a material-dependent local-field factor [50]. Moreover, the different multipolar orders are described by different susceptibilities [13].

In nanostructures including ordered arrays of nanoparticles (such as the ones discussed in this paper) the electromagnetic fields, material properties, and nonlinear sources can, however, vary over the scale of a wavelength or less [51, 52]. The nonlinear responses must then be integrated over the entire structure. Whereas this can be done phenomenologically for structures of high symmetry, it is presently intractable for more complicated geometries. Moreover, higher multipoles such as magnetic dipoles, electric quadrupoles, etc. may also contribute to the macroscopic response.

To avoid the nanoscale difficulties, we have introduced a macroscopic nonlinear response tensor (NRT), which operates on the level of input and output fields [49]. In the NRT formalism for SHG, the input is the vector amplitude of the exciting field and the output is that of the frequency-doubled field. Formally, the NRT tensor relates a specific polarization component of the SH field to components of the fundamental field:

$$E_i(2\omega) = \sum_{jk} A_{ijk} E_j(\omega) E_k(\omega), \tag{1}$$

which bears resemblance to the expression for the SH source polarization in the susceptibil-

#97124 - $15.00 USD Received 6 Jun 2008; revised 6 Oct 2008; accepted 7 Oct 2008; published 13 Oct 2008
(C) 2008 OSA

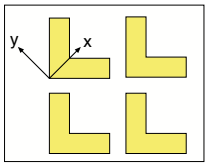

Fig. 1. An array of L-shaped particles and the associated coordinate system.

ity formalism [50]. However, important conceptual differences are that the measurable signal field, and not the nonlinear source, appears on the left-hand side of Eq. (1), and that the NRT implicitly includes the contributions from all different multipolar nonlinear sources.

The NRT is therefore a convenient way to describe the measurable optical responses without worrying about the electromagnetic field distribution and material inhomogeneities in the nanoscopic structures or the complicated interactions and interferences occurring on the nanoscale. A major limitation of the NRT is that it is specific to a given experimental geometry, rather than to the sample itself. This can be used to our advantage, though. Comparison of NRTs determined under different experimental conditions provides valuable insight to the physical processes at the nanoscopic level [47].

A particularly relevant experimental geometry for the NRT formalism is when an essentially two-dimensional sample is placed at normal incidence with respect to the exciting fundamental beam. We can then use the same coordinate basis to describe both the sample and the polarization states of the exciting and signal beams. This geometry thus allows us to apply electric-dipole-like selection rules to determine the allowed polarization combinations of the input and output fields.

In the present Paper, we apply the NRT formalism to a regular array of L-shaped nanoparticles on a substrate. The shape suggests a set of in-plane coordinate axes, where the *x*-axis bisects the arms of the L (c.f. Fig. 1). This structure belongs to the C_{1h} symmetry group, for which the only symmetry operation is reflection through the *xz*-plane. The in-plane NRT components and whether they are allowed (for the ideal L-shape) are listed in Table 1.

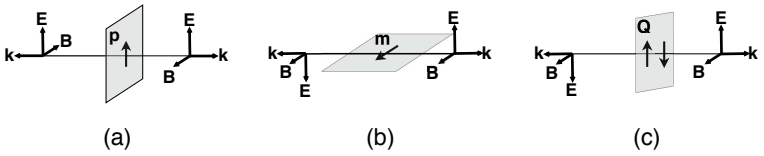

Fig. 2. Illustration of the differences in radiative properties of (a) electric dipole *p*, (b) magnetic dipole *m* and (c) electric quadrupole Q. Vectors *k*, *E*, and *B* are the wavevector, electric field, and magnetic field, respectively.

The NRT formalism can be connected to multipole effects by considering the far-field emission patterns of different multipole sources. We measure coherent SH signals, which dominate the response of the surface-like samples used and give rise to strong signals only in the transmitted and reflected directions. The radiated far fields of an electric dipole, a magnetic dipole, and an effective electric quadrupole formed from a pair of spatially-separated electric dipoles are shown in Fig. 2. The radiative properties of the various multipoles in the transmitted and reflected directions are seen to lead to opposite interference effects in the two directions. Moreover, we may expect the strength of the various types of sources to depend on the polarization of the driving field. The response will then exhibit polarization-dependent interference effects, allowing us to distinguish the different multipolar contributions to the overall SHG response,

#97124 - $15.00 USD Received 6 Jun 2008; revised 6 Oct 2008; accepted 7 Oct 2008; published 13 Oct 2008
(C) 2008 OSA

even when the absolute signal levels cannot be calibrated.

To quantify the relative importance of different multipoles to the SH response, we assume that each NRT component consists of two parts—symmetric (s) and antisymmetric (as)—which transform differently with the choice of detection arm:

$$A_{ijk}^{\mathrm{T,\,R}} = A_{ijk}^{\mathrm{s}} \pm A_{ijk}^{\mathrm{as}}, \tag{2}$$

where superscripts "T" (+ sign) and "R" (- sign) refer to the transmitted and reflected directions. Thus,

$$A_{ijk}^{\mathrm{s}} = \frac{1}{2}\left(A_{ijk}^{\mathrm{T}} + A_{ijk}^{\mathrm{R}}\right), \quad A_{ijk}^{\mathrm{as}} = \frac{1}{2}\left(A_{ijk}^{\mathrm{T}} - A_{ijk}^{\mathrm{R}}\right). \tag{3}$$

The symmetric part originates from the electric dipole, whereas the antisymmetric part is attributed to magnetic-dipolar or electric-quadrupolar origins (cf. Fig. 2).

Our experiments are thus based on comparing the relative values of the NRT components in the reflected and transmitted directions. In order to determine them for each direction separately, we note that at normal incidence the *x*- and *y*-polarized SH signals are

$$E_i(2\omega) = A_{ixx}E_x^2(\omega) + A_{iyy}E_y^2(\omega) + 2A_{ixy}E_x(\omega)E_y(\omega); \quad i = x,y, \tag{4}$$

where the factor of 2 in the last term accounts for the degeneracies $A_{iyx} = A_{ixy}$.

In order to relate both the relative phases and magnitudes of *x*- and *y*-polarized SH sources (components A_{xjk} and A_{yjk}), we detect both mixed and pure *x*- and *y*-polarized signals. Therefore, because we measure intensity rather than electric field, the model function we use to describe the SH signals becomes:

$$\begin{aligned} I_\delta(2\omega) \quad = \quad & \Big|\left(A_{xxx}\sin\delta + A_{yxx}\cos\delta\right)E_x^2(\omega) + \left(A_{xyy}\sin\delta + A_{yyy}\cos\delta\right)E_y^2(\omega) + \\ & 2\left(A_{xxy}\sin\delta + A_{yxy}\cos\delta\right)E_x(\omega)E_y(\omega)\Big|^2, \end{aligned} \tag{5}$$

where the angle δ describes the azimuthal orientation of the analyzer with respect to the *x*-axis of the sample. We emphasize that Eq. (5) forms the basis for determining the relative complex values of the NRT components for each detection direction separately. Although the absolute phase of the components remains unknown, their relative magnitudes are determined unambiguously, which provides important information regarding the origin of the nonlinear response.

3. Experimental

Our sample consists of an array of L-shaped metal nanoparticles, prepared using electron-beam lithography [46]. The linewidth of the L's is ~ 100 nm, the arms are ~ 200 nm long, and the gold layer is 20 nm thick. The particles are covered with a 20 nm layer of fused silica. They are arranged in a regular array on a fused silica substrate, with an array spacing of 400 nm and an active area of 1×1 mm^2. The sample is strongly dichroic [48], see Fig. 3.

Our experimental setup is shown in Fig. 4. A train of femtosecond pulses from a Nd:Glass laser system (Time-Bandwidth Products GLX-200; 200 fs pulse duration, 1060 nm center wavelength, 350 mW average power, 82 MHz repetition rate), is chopped and weakly focused onto the sample with a spot size of ~ 200 μm. The polarization of the fundamental beam is controlled with a half wave plate (HWP) and a quarter wave plate (QWP). The HWP is used to set the azimuthal angle of the initial linear polarization, and the QWP, mounted in a motorized rotation stage, modulates the polarization continuously. We can thus excite the sample with different elliptical polarization states while observing the SH responses, which is beneficial for increasing the reliability of the data analysis [53].

#97124 - $15.00 USD Received 6 Jun 2008; revised 6 Oct 2008; accepted 7 Oct 2008; published 13 Oct 2008
(C) 2008 OSA

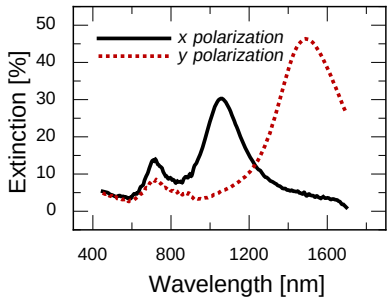

Fig. 3. Measured optical density of our sample. Note that *x*-polarization is in resonance with the fundamental wavelength of our laser, 1060 nm.

Figure 4(b) depicts the experimental geometry [47]. We must tilt the sample slightly off-normal with respect to the fundamental beam ($\alpha < 2^{\circ}$) to be able to detect the reflected SH signal without compromising its polarization state. Only *s*-polarized (normal to the plane of incidence) SHG is detected, which guarantees that differences in transmission and reflection cannot arise from interference between dipole sources directed along the normal to the sample (z) and along the in-plane direction (e.g., x). These dipole sources would interfere differently for *p*-polarized (in the plane of incidence) detection [12]. To distinguish *x*- and *y*-polarized contributions to SHG, we rotate the sample about its surface normal while maintaining the analyzer fixed normal to the plane of incidence. We detect the SH intensity as a function of the fundamental field polarization with a photo-multiplier tube connected to a lock-in amplifier referencing the chopper frequency.

The NRT components are extracted from the measurement data by nonlinear least-squares optimization [54]. The *x*-, *y*-, and $x+y$-polarized SH datasets from a given measurement arm are combined and fitted simultaneously to Eq. (5). Simultaneous fitting is performed to decrease both the dependence of the fit result on initial values assigned to the fit variables and the relative importance of any one individual dataset to the combined-fit result.

As individual data sets have not been mutually calibrated for signal intensities, we assign to each a real scaling coefficient representing polarization-dependent losses in the optical setup. In order to fit multiple data sets to the same function we need to keep careful track of the angles of the waveplate axes with respect to the reference axis and the sample's azimuthal rotation angle. The model function then reconstructs the electric field components E_x and E_y (in the sample frame) by applying appropriate coordinate transformations to the Jones matrices [55]

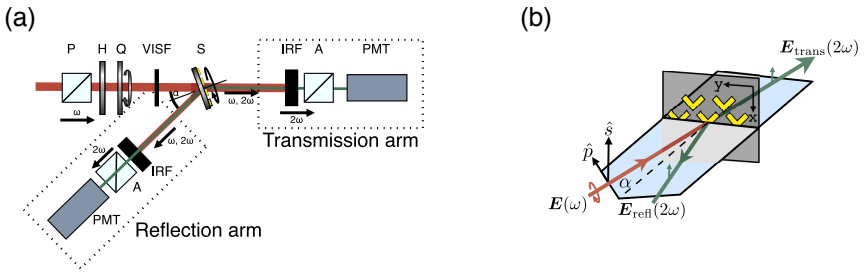

Fig. 4. (a) Experimental setup. P = polarizer; H = half wave plate; Q = quarter wave plate; VISF = long-wavelength pass filter; S = the sample; IRF = short-wavelength pass filter; A = analyzer; and PMT = photo-multiplier tube. (b) The experimental geometry.

#97124 - $15.00 USD Received 6 Jun 2008; revised 6 Oct 2008; accepted 7 Oct 2008; published 13 Oct 2008
(C) 2008 OSA

representing the effects of the waveplates on the fundamental field.

Before the actual measurements, we addressed possible sources of errors and uncertainties that might affect our results. First, the array period is sub-wavelength for both the fundamental and SH wavelengths in free space. However, the period is larger than the SH wavelength in the substrate. Therefore, some SH light may be emitted into the substrate, but at such a large angle that it cannot escape the substrate, which leaves only the zeroth diffraction order to contribute to the propagating SH signals. In addition, our technique is not based on absolute signal levels and is therefore not compromised by possible emission into the substrate.

Although our incidence angle is very close to normal and only *s*-polarized light is detected, the polarization of the fundamental beam can contain a small *z*-(sample normal) component. The effect of this possibility was studied by repeating measurements at an incidence angle of approximately 2α (cf. Fig. 4). We found no change in the features of the obtained lineshape, implying that for shallow incidence angles, the SH response does not have an appreciable *z*-dependence. The sensitivity to the alignment of the analyzer was tested by rotating it $\pm 1^{\circ}$ away from *s*-polarization, which resulted in no appreciable change in the lineshape, only a slight decrease of the overall magnitude. As we have measured optical activity at the fundamental wavelength from similar samples [56], we also tested for polarization effects at the SH wavelength by illuminating the sample with linearly-polarized light at the SH wavelength. It was found that the polarization was virtually unchanged at the SH wavelength, thereby excluding the possibility of optical activity.

4. Results

The experimental data and their simultaneous fits to the six in-plane NRT components are shown in Fig. 5. It can be immediately seen that the experimental data contains differences between the transmission and reflection arms, which already provides qualitative evidence of multipole contributions to the response. The experimental data and fit results have been normalized to the maximum intensity in each plot in order to accommodate differences in the light collection efficiencies of the two detection arms, as well as any polarization-dependent losses. These slight differences have no influence on the interpretation of our results because our technique does not rely on absolute signal intensities. Note, however, that the absolute levels of the various signals are very different. In particular, the absolute signal intensities in Figs. 5(e) and 5(f) are significantly weaker than those in Figs. 5(a)-(d). The absolute signal level in Fig. 5(f) is close to the noise level of the detector in the weakest parts of the signal. Note that the noisy signals are not necessary to solve the NRT components, however, they are seen to have overall compatibility with the other data sets.

Table 1. In-plane NRT components for (ideal) L-shaped nanoparticles and experimental values extracted from Eq. (5)

		Transmission		**Reflection**	
	Allowed	**Value**	**Magn.**	**Value**	**Magn.**
A_{xxx}	YES	1.00	1.00	1.00	1.00
A_{xyy}	YES	0.64-0.35i	0.73	0.44-0.39i	0.59
A_{xxy} [1]	NO	0.22-0.05i	0.23	0.15-0.10i	0.18
A_{yxx}	NO	0.15-1.42i	1.43	-0.06-0.83i	0.83
A_{yyy}	NO	-0.01+0.13i	0.13	-0.04+0.20i	0.20
A_{yxy} [1]	YES	-0.49-0.24i	0.55	-0.27-0.11i	0.29

[1] The degeneracies $A_{ixy} = A_{iyx}$ have been omitted.

#97124 - $15.00 USD Received 6 Jun 2008; revised 6 Oct 2008; accepted 7 Oct 2008; published 13 Oct 2008
(C) 2008 OSA

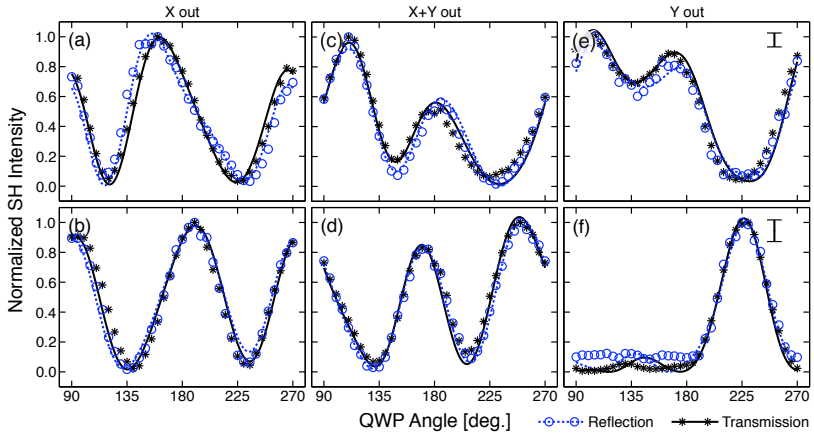

Fig. 5. Measured lineshapes. Asterisks: transmission SH data; circles: reflection SH data. Solid and dashed lines are fits to Eq. (5) in transmission and reflection geometries, respectively. The starting linear polarization was *p* for (a), (c), and (e), and *s* for (b), (d), and (f). QWP values 135° and 225° correspond to left- and right-hand circular polarizations, respectively. Estimations of the relative uncertainties due to detector noise are indicated with the symbol size, except for those measured in reflection geometry (dashed line) in plots (e) and (f), where the uncertainties are indicated with the errorbars.

The fitted values of the NRT components relative to A_{xxx} are shown in Table 1. A_{xxx} has been normalized to unity in both directions for reasons to be explained shortly. The values A_{xyy} and A_{xxy}, are seen to exhibit quantitative but not qualitative differences compared to Ref. [47] where those components were determined from a single measurement (Note that the definitions of A_{xxy} between Ref. [47] and present work differ by a factor of two). We attribute the differences to the fact that we used more data in the fitting, forcing the same set of coefficients to describe more than one experiment, therefore de-emphasizing the relative importance of any single data set. Considering that the same set of coefficients describes six different measurements, the overall fit quality is very good. In transmission, the SH responses are dominated by a symmetry-forbidden component, A_{yxx}, which is also resonant at the fundamental wavelength. We remind that both allowed and forbidden components can have dipolar and higher-multipolar contributions. However, chirality is closely connected to multipole effects. Hence, large components associated with chiral symmetry breaking could also have a strong multipolar character.

To assess the importance of the higher-multipole contributions, we note that the data sets have been fitted to Eq. (5) for each direction separately. To separate the symmetric and antisymmetric parts, we need an additional assumption that connects the results in the two directions. We therefore assume that the component A_{xxx}, which is allowed for the ideal structure and has a plasmonic resonance at the fundamental wavelength of 1060 nm, is of purely electric-dipole origin. This component must then be equal for both directions and is normalized to unity. The relative differences with the remaining coefficients for the transmitted and reflected directions can then be taken as a measure of the importance of higher-multipole contributions. We define the multipolar contribution γ of a given component as the ratio of the magnitudes of its antisymmetric and symmetric parts:

$$\gamma_{ijk} = \left| \frac{A^{\mathrm{as}}_{ijk}}{A^{\mathrm{s}}_{ijk}} \right| . \tag{6}$$

We acknowledge that assuming A_{xxx} to be of purely dipolar origin is not completely justified

#97124 - $15.00 USD Received 6 Jun 2008; revised 6 Oct 2008; accepted 7 Oct 2008; published 13 Oct 2008
(C) 2008 OSA

at present and that it may also include some higher-multipolar character. We therefore also analyzed our data under the conditions where each tensor component was separately assumed to have only dipolar character. In addition to the earlier mentioned physical grounds for using A_{xxx} as the purely dipolar component, we found that this choice also minimizes the γ ratio of the other NRT components.

Table 2. Multipolar contributions of NRT components.

	A^{s}	A^{as}	γ (%)
A_{xxx}	1.00	0.00	0
A_{xyy}	0.54-0.37i	0.10+0.02i	15
A_{xxy}	0.19-0.08i	0.03+0.02i	20
A_{yxx}	0.04-1.12i	0.10-0.30i	28
A_{yyy}	-0.03+0.17i	0.01-0.03i	21
A_{yxy}	-0.38-0.17i	-0.11-0.07i	31

5. Phenomenological interpretation

The results of Table 2 show that the largest relative multipolar contributions occur for the symmetry-allowed component A_{yxy} ($\gamma_{yxy} = 0.31$) and the symmetry-forbidden A_{yxx} ($\gamma_{yxx} = 0.28$). However, the symmetry-forbidden component has clearly the largest absolute value of the multipolar contribution. This suggests that the higher multipolar contributions are closely associated with chiral symmetry breaking of the sample. A possible source of such symmetry breaking is asymmetrically distributed structural defects that remove the reflection symmetry of the sample with respect to the *xz*-plane. In the following, we present a simple phenomenological model that shows how dipolar elementary sources associated with non-equivalent defects at opposite lateral sites of the particles [Fig. 6(a)] may give rise to dipolar and effective quadrupolar sources that are forbidden for ideal particles.

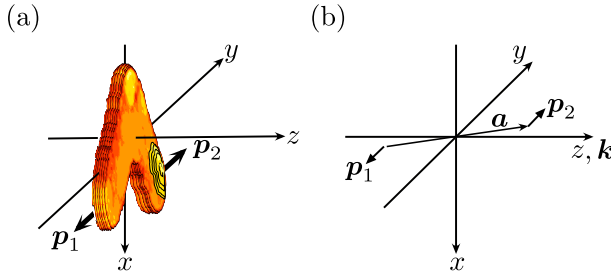

Fig. 6. (a) Visualization of L-shaped particle where laterally opposite sides have non-equivalent defects. (b) Example of an effective quadrupole formed from two displaced opposite dipoles.

To illustrate the basic idea of the model, we first consider a system of two dipoles with their dipole moments pointing in opposite directions along the *y*-axis, i.e., $p_1 = -p$ and $p_2 = p$, where $p = py$. In addition, we assume that that the dipoles are separated by a small vector $a = a_x x + a_y y + a_z z$, and consider emission in the direction $k = kz$ parallel to the *z*-axis [Fig. 6(b)]. Such a system cannot give rise to dipolar emission. Instead, the system acts as an effective quadrupole source. In the dyadic notation, this quadrupole is proportional to

$$\mathrm{Q} \propto ap + pa, \tag{7}$$

#97124 - $15.00 USD Received 6 Jun 2008; revised 6 Oct 2008; accepted 7 Oct 2008; published 13 Oct 2008
(C) 2008 OSA

from which it follows that the nonzero components of the quadrupole moment tensor in this geometry are $Q_{xy} = Q_{yx} = pa_x$, $Q_{yy} = 2pa_y$, and $Q_{zy} = Q_{yz} = pa_z$.

The electric field emitted by such a source into the far field in direction $k = kz$ is then proportional to

$$E_{\mathrm{Q}} \propto i(k \cdot \mathrm{Q}) = i(k \cdot a)p + i(k \cdot p)a, \tag{8}$$

which in the present geometry reduces to

$$E_{\mathrm{Q}} \propto i(k \cdot a)p = ika_z py = ikQ_{zy}y. \tag{9}$$

This result is seen to depend on the retardation of the two dipolar sources along the direction of emission, i.e., on a_z. Note that the directions of emission $k = kz$ have opposite signs. As a consequence, the emitted wavelets will have opposite phases in the two directions (Fig. 2).

We next consider the situation that is relevant to our experiment and where the laterally opposite sides of the L have non-equivalent defects [Fig. 6(a)]. We assume that the defects act as localized dipolar sources of SH radiation. To understand the origin of the forbidden A_{yxx} signal, we consider the *y*-polarized parts of the sources. Because the defects are non-equivalent, their dipole moments p_1 and p_2 can be unequal. In addition, the sources can be localized at different z positions on the particles. To be specific, we take the sources to be localized at $z = \pm a_z/2$. The total far field emitted by such dipolar sources is then proportional to

$$E \propto p_1 \exp(-ika_z/2) + p_2 \exp(ika_z/2), \tag{10}$$

which fully accounts for the phases of the two wavelets. In the spirit of the multipole approach, we expand the exponential to lowest order with respect to the small separation to obtain

$$E \propto p_1 + p_2 + (p_2 - p_1)ika_z/2, \tag{11}$$

whose second term clearly behaves as emission from an effective quadrupole where the two dipoles are mutually retarded. For an ideal L shape with reflection symmetry with respect to the *xz*-plane, the forbidden SH signals would be associated with equal and opposite *y*-polarized sources ($p_1 = -p_2$) at equal heights ($a_z = 0$). Therefore, neither dipolar nor quadrupolar effects can give rise to forbidden signals from symmetric samples. In the presence of symmetry breaking, on the other hand, both dipolar and quadrupolar signals can exist simultaneously.

We emphasize that in the above phenomenological model, the elementary SH wavelets arise from localized dipolar sources distributed to different locations on the particles. The variations in such localized sources, however, must be in agreement with the overall symmetry properties of the sample. Surface defects on the particles provide a particularly obvious mechanism for such localized sources. Asymmetric distribution and/or orientation of such defects on the opposite sides of the particles can give rise to mutually imbalanced local sources whose interference leads to forbidden signals. Consequently, the localized sources modify the values of the NRT components and give rise to their parts with dipolar and quadrupolar characters. In our experiment, the excitation of the SH sources p_1 and p_2 depends on the polarization of the fundamental field, which thereby accounts for the polarization-dependent interference between dipolar and multipolar emission. In the above discussion we have emphasized the use of the phenomenological model in accounting for the forbidden signals and their dipolar and quadrupolar parts. However, depending on the properties of individual defects, they can also contribute to the allowed signals. Such contributions and their dipolar and multipolar parts can easily be accounted for with the same approach.

6. Conclusions

We have presented a comprehensive multipolar tensor analysis of second-harmonic radiation from a regular array of noncentrosymmetric L-shaped gold nanoparticles. Our measurements

#97124 - $15.00 USD Received 6 Jun 2008; revised 6 Oct 2008; accepted 7 Oct 2008; published 13 Oct 2008
(C) 2008 OSA

were based on fundamental differences in the radiative properties of electric dipoles and higher multipoles in two opposite directions. For coherent SH signals, these differences result in opposite interference effects in the reflected and transmitted signals. Such effects were described by expressing the components of the nonlinear response tensor of the sample as a sum of symmetric and antisymmetric parts between the two directions, which correspond to the dipolar and higher-multipolar parts of the tensor component, respectively.

In addition to reaffirming our earlier results regarding the importance of multipole contributions, we found that the nonlinear response is dominated by a tensor component associated with chiral symmetry breaking in the sample. This tensor component also exhibits a strong multipolar character. The close relation between the chiral symmetry breaking and strong multipole effects was explained by a phenomenological model where dipolar and quadrupolar SH emission arises from interference between the retarded SH wavelets emitted by defects located at the two opposite sides of the particle. The facts that a symmetry-forbidden coefficient is strongest in magnitude and has a strong multipolar contribution thus corroborate the interpretation that one of the major contributors to the optical response of the present sample is structural defects, which break the symmetry and make multipolar contributions to the SH response important. However, the role of defects need not be limited to forbidden signals, and their dipolar and quadrupolar contributions to the allowed signals can be explained by a similar approach.

We note that in the present work we were able to resolve the dipolar and multipolar contributions in the emission of SH radiation. In the future, it will be important to address the role of higher-multipole contributions also at the fundamental frequency. In addition, it will be interesting to correlate the magnitude of higher-multipole effects to the surface quality of the samples once systematic variation of the quality becomes possible. Finally, for the present sample, the laser was resonant with one of the plasmonic resonances of the sample, which can give rise to complicated phases of the determined tensor components. Our technique properly determines the relative complex values of the tensor components, but not their absolute phases. It will therefore be important to determine of the various multipole contributions to the nonlinear response also under off-resonant conditions, where the phase relations are expected to be simpler.

Acknowledgments

This work was supported by the Academy of Finland (113245, 114913, 115781, 118357, 209806) and by the Nanophotonics Research and Development Program of the Ministry of Education of Finland. SK acknowledges support from the Graduate School of Tampere University of Technology. We gratefully acknowledge Konstantins Jefimovs for sample preparation.

#97124 - $15.00 USD Received 6 Jun 2008; revised 6 Oct 2008; accepted 7 Oct 2008; published 13 Oct 2008
(C) 2008 OSA